Wahyu Widhi Dyatmika

Towards the Application of Generalised Richardson Extrapolation in Spanwise Oscillating Wall Flow Control Analysis

SCHOOL OF AEROSPACE, TRANSPORT AND MANUFACTURING
Computational Fluid Dynamics

MSc
Academic Year: 2023 - 2024

Supervisor: Tamás Jozsa
25th August 2023

SCHOOL OF AEROSPACE, TRANSPORT AND MANUFACTURING
Computational Fluid Dynamics

MSc

Academic Year: 2023 - 2024

Wahyu Widhi Dyatmika

Towards the Application of Generalised Richardson Extrapolation in Spanwise Oscillating Wall Flow Control Analysis

Supervisor: Tamás Jozsa
25th August 2024

This thesis is submitted in partial fulfilment of the requirements for the degree of MSc

Academic Integrity Declaration

I declare that:

- the thesis submitted has been written by me alone.
- the thesis submitted has not been previously submitted to this university or any other.
- that all content, including primary and/or secondary data, is true to the best of my knowledge.
- that all quotations and references have been duly acknowledged according to the requirements of academic research.

I understand that to knowingly submit work in violation of the above statement will be considered by examiners as academic misconduct.

Abstract

Acknowledgement

Contents

List of Figures

List of Tables

List of Symbols and Abbreviations

Abbreviations

CFD	Computational Fluid Dynamics
CF	Channel Flow
DNS	Direct Numerical Simulation
GREP	Generalised Richardson Extrapolation
ISA	Inner-Scale Actuation
LES	Large-Eddy Simulation
NPS	Net Power Saving
NR	Normalised Resolution
OSA	Outer-Scale Actuation
PF	Pipe Flow
RANS	Reynolds Averaged Navier Stokes

Variables (Latin Letters)

E	Energy
e	Vector component
g	Gravitational vector
h	Height
L_o	Integral Length Scale
n	Variable for showing time step
P	Pressure
Re	Reynolds number
t	Time
u	Velocity vector
$u.\ v, w$	Streamwise, wall-normal, and spanwise velocity, respectively
x, y, z	Streamwise, wall-normal and spanwise direction, respectively

Variables (Greek Letters)

δ	Characteristic length
η	Kolmogorov length scale
κ	Wave number
λ	Minimal flow length
ν	Kinematic viscosity
μ	Dynamic viscosity
ρ	Density
ϕ	Transported quantity

Subscripts and Superscripts

$*$	Intermediate values
$+$	Wall-normal value
τ	Viscous quantities

1 Introduction

In the subject of fluid dynamics, flow control can massively influence the performance of the flow around or inside an object. Designing a flow control method requires intricate understanding of flow behaviours such as dynamics and turbulence. Designing a proper flow control can be essential for maximising the efficiency of the system.

1.1 Motivation

Climate change has been a driving factor for engineering design in the modern world [1]. The changes in climate pattern has proven to be detrimental to human and other living being. One of the causes of the climate change is the emission of energy generation process, such as carbon dioxide [2]. However, the need of creating more energy is indispensable as human population grows continuously, with energy requirement predicted to reach more than the triple of global energy requirement today [3]. This requires engineers to create a high performance solution with a consideration of efficiency in its operations. In aerospace sector, this approach is also used as the sector creates 2% of the total global emission, which is the largest among other means of transportation [4]. Generally in aerospace sector, high efficiency value can be reached by minimising drag, which generated from the viscous drag, as shown in Figure 1. The viscous drag can be practically reduced in a controlled manner using flow control strategies, offers a solution for a sustainable aerospace future [5].

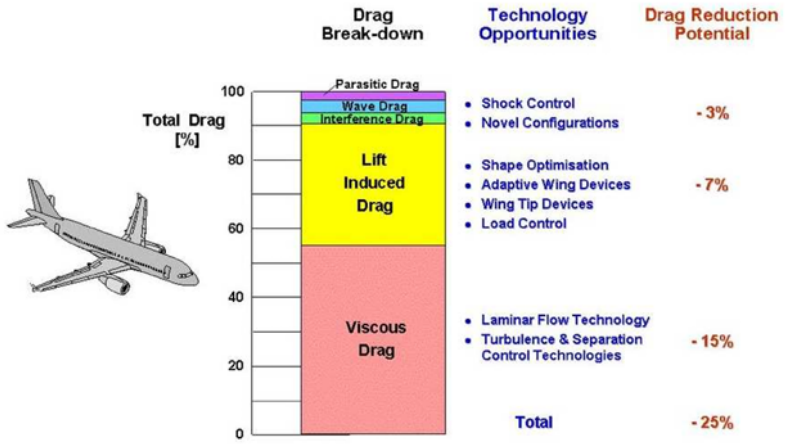

Figure 1: Drag and Reduction Potential in a General Aircraft [5]

Fluid flow control has been a major topic in fluid dynamics. Fluid flow control strategies have been implemented in various areas, such as aerospace, wind energy sector, industrial process designs, and water management [6]. The development of flow control methods was born from the understanding of the presence of turbulence in a fluid flow. Turbulence

in a moving flow can generally be denoted by the chaotic behaviour of the fluid [7], typically in the form of eddies or vortices. The interaction of the flow with itself, along with the solid object nearby can produce drag, which reduces the flow velocity and its ability to transport its properties [8]. In most systems, the drag can be detrimental as it can reduce the efficiency of the system. Because of that, flow control strategies are introduced to force the fluid to move in a regulated behaviour to decrease the drag produced in the system.

Currently, multiple strategies and approaches towards an efficient flow control system are studied. One of recent studies [9] suggests that an active flow control strategy in the form of spanwise wall oscillations can generate a positive net power saving value for high Reynolds number regimes. With the finding, a pathway for an industrial-wide application of oscillating wall flow control can be opened and hence a further studies are needed.

In order to further expand the spanwise wall oscillation flow control strategy, understanding the turbulence in the flow is of utmost importance, especially in the near wall region. Turbulence is the chaotic nature of a fluid flow, caused by "a complex interplay of multiple flow patterns occurring simultaneously, making difficult to model and predict accurately" [10]. Therefore, intricate physics modelling is generally required to completely simulate the turbulence in the flow, which growingly expensive in terms of computational cost as the Reynolds number increases [11]. In this paper, direct numerical simulation (DNS) is introduced as a solution for high-fidelity simulation, incorporating generalised Richardson extrapolation to make the analysis time-efficient. This paper will mainly utilises ARCHER2 HPC environment for generating the data to create more efficient simulation.

1.2 Literature Review

1.2.1 Physics of Wall Bounded Flow Turbulence

Turbulence can be defined as the swirling motion that happened randomly in the fluid flow [12]. Due to its randomness, turbulence phenomena can sometimes be too complicated and difficult to comprehend [13]. Therefore, most turbulence studies are focused on understanding the coherent structures, which are the regions with recognisable concentrated vorticity [14]. As seen in Figure 2, there are common structures in the flow region near the wall that is identifiable. The most prominent structure is the hairpin vortex, which indicated by a raising arch head with two streamwise-oriented legs [15].

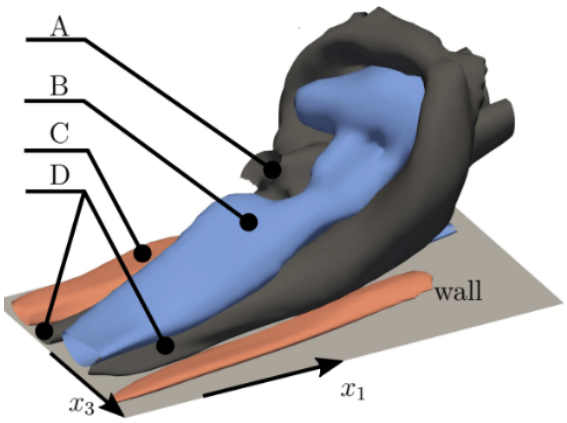

Figure 2: Near Wall Coherent Structures: A) Hairpin Vortex ; B) Low momentum region; C) high momentum region; D) counter-rotating quasi-streamwise vortices [16]

Several researches, such as the studies made by Wang [15] and Alfonsi [17] explained how the hairpin vortices generated. First, the legs of the hairpin vortices, which consist of two quasi-streamline, counter-rotating vortices are interacted with each other. These vortices rises to the area with lower shear magnitudes, which decreases the vorticity magnitude. With the opposing rotational direction, the coalescence of two vortical structures are occurred and the hairpin vortices are generated. Inside the vortex, low momentum region is generated. Conversely, the high momentum region is generated outside the two counter-rotating vortices.

Other than the physical structures, the spectral analysis is also commonly conducted to understand the turbulence phenomena. Generally, spectral analysis involves analysing the turbulence through the wave energy distribution in the structures [18]. In order to visualise the energy distribution, the Kolmogorov spectrum is used, as shown in the Figure 3.

Based on Brennen [19], there are 3 main regions in the spectrum. The first is the integral region, or commonly known as the energy containing range. This characterises the overall size of the largest eddies, which contains the energy in the flow. These large scale structures are responsible for transfering energy to the from the external forces to the smaller structures in the turbulent flow. The energy is then cascades to the smaller scales through the inertial region. The energy spectrum in this region follows a power law distribution:

$$E(k) \propto k^{\frac{5}{3}} \tag{1}$$

Where k is wave number. Afterwards, the energy cascades to the smallest scales, which are in the Kolmogorov scales. In this scales, the viscosity dominates and the kinetic energy is transfered to heat energy.

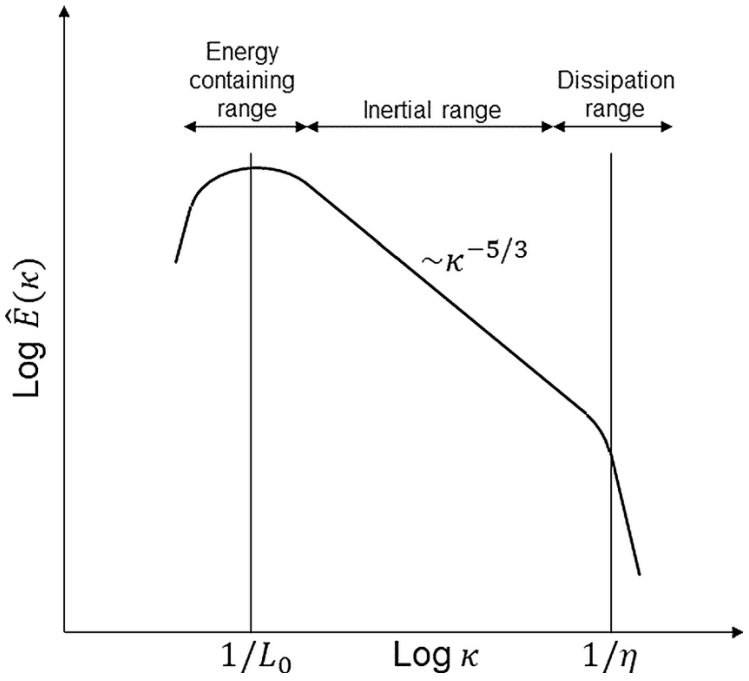

Figure 3: Typical Energy Spectrum in a Flow [20]

1.2.2 Spanwise Oscillating Wall Flow Control

Flow control can be defined as the method of altering the flow to a desired state or path [21]. Typically, there are two types of flow control methods, as stated by Ricco [22]. The first method is the passive flow control, which requires no actuation or movement in the system, thus no external energy required to control the fluid flow. The second method is the active flow control. Contrary to its passive counterpart, the active flow control requires energy to actuate a motion in a flow.

Due to the certain energy consumption, most of the study regarding active flow control are circulated around the strategy to create a motion that has a positive net power saving. The same trend has been observed for spanwise oscillating wall method, which requires actuation to create an oscillation in the near wall region. The concepts and methods are documented in Table 1.

Table 1: Experimental and Computational Studies of Spanwise Oscillating Wall Flow Control

References	Geometry	Methodology	Reynolds Number	$\mathbf{NPS}_{max}$ (%)
Marusic et al. (2021) [9]	CF	Experimental: Hot-wire anemometry Computational: LES (dynamic Smagorinsky)	Re_τ = 6000 Re_τ = 12800	∼7 ∼2
Gatti and Quadrio (2016) [23]	CF	Computational: DNS	Re_τ = 200 Re_τ = 1000	5.3 ± 0.24 3.9 ± 0.31
Quadrio et al. [24]	CF	Computational: DNS	Re = 4760	5
Auteri et al. (2010) [25]	PF	Experimental, with DNS comparison from [24]	Re = 4760	17
Viotti et al. (2009) [26]	CF	Computational: DNS	Re_τ = 200	23
Chandran et al. (2023) [27]	CF	Experimental: Drag Balance and Hot Wire Anemometry	$4500 \leq Re_\tau \leq 150000$	ISA: -40 OSA: 5-10
Deshpande et al. (2024) [28]	CF	Computational: DNS	$Re_\tau \approx 300$	Not reported
Nguyen et al. (2021) [29]	CF (with square bar)	Computational: DNS	Re_τ = 218	0.8
Ricco et al. (2012) [30]	CF (rough wall)	Computational: DNS	Re_τ = 200	Not reported

The key trend from the results is the NPS value is dependent from various factors. It is apparent from the studies that the NPS value of of the flow control decreases as the Reynolds number increases [23] [24]. Other than that, the net power saving also relies on the wave function applied. From the studies, it can be seen that the net power saving is positive when the wave function of the oscillating wall matches the large-scale eddies inside the flow [9][27].

Based on the table, a simple channel flow is the most common base case to test the effectivity of flow control. This is due to the simplicity of the flow modelling as the case only has two wall surface, generally placed on the top and the bottom of the domain. The domain surfaces on the side are assumed to be free surfaces [31]. To the boundary condition assignment, the effect of the wall in the flow will be easier to analyse without having to take account the wall perpendicular to the wall of interest.

1.2.3 Turbulence Modelling

Solving turbulence is required in order to create a good model of a fluid flow. This is because turbulence is highly related to the transport of mass, energy, and other values in the flow [32]. However, variety in the temporal and spatial scale of turbulence oftentimes requires high computational power [33]. To alleviate the excessive computational power, turbulence modelling is often used, generally in the form of Reynolds Averaged Navier Stokes (RANS) [34]. However, due to the nature of the modelling, some simplifications leads to information loss, especially regarding the energy cascade to the small scales [35]. Other approach that can be done is using the Large Eddy Simulation (LES). LES method solves large eddies directly, but uses modelling to solve the small eddies [36]. This way, high accuracy can be obtained for the large structures, while maintaining low computational expenses. However, similar to RANS modelling, inaccuracy can occur in small-scale turbulence [37].

In cases where the effect of small-scales turbulence are heavily considered, turbulence modelling is fully disregarded. This means that the Navier-Stokes equations are directly solved [38]. These method of solving the fluid flow is termed Direct Numerical Simulation (DNS). Ideally, DNS should be performed with spatial resolution at least as large as the Kolmogorov scale, which the smallest eddies that can be produced by the flow [39]. However, the fine grid resolution will make the analysis prohibitively expensive. Therefore, lower resolution usually preferred to DNS methods.

1.2.4 Grid Convergence and Generalised Richardson Extrapolation

A certain confidence to the result must be the base of a computational simulation. The confidence is needed so the result can be applicable and have a good degree of reflecting

the physical phenomena of the problem. In CFD, the confidence is build by proving the consistency of the result using grid convergence study (GCS), which introduced by Roache [40]. Grid convergence study involves a minimum of 3 different simulation model with resolution variation, generally named as coarse, medium, and fine model [41]. The resolution of the models are variated using the following relation

$$N = 2^n m + 1 \tag{2}$$

The domain settings may change the value of the results. The finer the settings is, the higher the quality of the results. However, finer results require high computational resources which limits the resolution of the model. To counter the problem. the Richardson extrapolation is usually used. Richardson extrapolation can be defined as the approximation of the ideal value of convergent value using [40]:

$$f_{h=0} \simeq \frac{4}{3} f_1 - \frac{1}{3} f_2 \tag{3}$$

However, most of the application of Richardson extrapolation are limited to the spatial convergence. The novel method of Richardson extrapolation includes temporal and domain size to determine the best resolution of a computational case.

1.2.5 Xcompact3d

The research mainly uses Xcompact3d to solve the fluid flow. Xcompact3d is a FORTRAN 90 based open-source software purposed to simulate incompressible fluid flows [42]. The software uses high order compact schemes [43], which utilises shortened version of high order schemes. This way, the analysis will still satisfy the need of high resolution of high-order schemes, while maintaining simplicity of low-order schemes [44], making the compact schemes a powerful and efficient tool to solve turbulence.

With the higher order schemes, the simulation can run high fidelity schemes to solve the viscous terms in the Navier-Stokes equation. The two models that are available to use in Incompact3d is Large Eddy Simulation (LES) and Direct Numerical Simulation (DNS) [43]. As the section 1.2.3 suggests, both methods are preferable when it comes to analysing turbulence in detail.

1.2.6 High Performance Computing

This study massively used HPC environments. Using HPC environments, the simulation can be accelerated into an extent with the increase of number of cores. Commonly, the acceleration is measured by the scalability parameter, which is the measure of the

simulation time affected by the problem size and number of workers or cores [45]. The scalability result is case-specific, thus every algorithm and different case will result a different scalability results.

Generally, there are two different methods of measuring scalability [46]. The first is the strong scaling, which expresses the solution time variation with the number of processors for a fixed total problem size. The strong scaling speedup is generally calculated using Amdahl law, which expressed as the following [47]:

$$speedup = \frac{1}{\left(\frac{t_{serial}+t_{parallel}}{N_{proc}}\right)} \tag{4}$$

The second method is the weak scaling. The scaling method expressed the solution time variation relating to the number of processors for a fixed problem size per processor. The weak scaling method utilises the Gustafson law [48], shown below.

$$scaledspeedup = t_{serial} + t_{parallel} \times N_{proc} \tag{5}$$

Another thing to consider when considering HPC services for simulation is the resources required. In ARCHER2, the resources allocated for the simulated is calculated in CU units, which is calculated as [49]:

$$CU = N_{nodes} \times t_{wallclock} \times N_{jobs} \tag{6}$$

And the cost required for the CU resources can also be calculated. The cost is calculated in pounds.

$$Cost = CU \times 0.20 \tag{7}$$

1.2.7 Knowledge Gap

Current spanwise oscillating wall flow control research lacks a thorough analysis in high Reynolds number. To conduct flow control studies using CFD, researchers must analyse turbulence in great depth, usually using LES or DNS analysis. This leads to high computational expenses. The expensiveness in the analysis is also exacerbated by the common practice of utilising a very large domain with a fine resolution, which makes the analysis in high Reynolds number particularly impossible. In this study, Generalised Richardson Extrapolation is introduced to decrease the computational requirement of the flow control analysis.

1.3 Aim and Objectives

The aim of this study is to analyse the effectivity of Generalised Richardson Extrapolation in numerical analysis of spanwise oscillating wall flow control.

With this aim, the objectives can be set as the steps to achieve the aim set. The objectives are set as follows:

- Introduce Xcompact3d in the HPC environment, paricularly CRESCENT2 and ARCHER2 environment
- Run a simple cylindrical test case in Xcompact3e
- Generate a channel flow grid as a main test case for the study
- Generate a generalised Richardson extrapolation by changing the spatial and temporal resolution
- Conduct flow simulations of the channel flow with and without spanwise oscillating wall flow control using DNS
- Generate and compare the time and ensemble averaging results using post-processing methods

1.4 Synopsis

The thesis is arranged to be in a form as follows. Section 2 provides the theoretical background and the methodology for the thesis. The governing equations, along with the supporting equations used in the numerical simulations are thoroughly explained. Moreover, the computational procedures, including geometry and mesh generations, simulations settings and post processing methods are introduced in this section.

Results obtained from the analysis is displayed in Section 3. The discussion is then served as the rationale of the result. Several figures and tables are displayed as a summary for the result and an aid for understanding the phenomena behind the flow condition. Section 4 presents the conclusions of the current study and recommendations for future studies.

2 Methodology

2.1 Flow Problem of Interest

2.1.1 Cylindrical Flow

As a test case for running the Xcompact3d, a simple cylindrical wake case is used. In this case, the a cylinder is subjected to a flow that creates a oscillating flow behind that are commonly known as the vortex shedding phenomenon. The parameters of the cylinder is set as default, given by the input example, shown in Table 2.

Table 2: Cylinder Wake Case Parameters

Re	x_{cyl}	y_{cyl}	r_{cyl}	u_b	ρ	ν
300	5	6	0.5	1	1	0.0033

It is worth noting that the cylinder wake case is only used as a means to check the result quality of Xcompact3d case. Therefore, the cylinder wake case will not be analysed as in depth as the channel flow cases.

2.1.2 Channel Flow

To understand the effect of oscillating wall flow control to the effect of the flow, a case must be formulated as an example case. Generally, the case used is a canonical flow problem, which the information and data are abundantly accessible and can easily compared to one and another. Therefore, the turbulence phenomena can be thoroughly examined. In this study, a simple double periodic channel flow problem is used to be analysed for the oscillating wall flow control problem. Double periodic channel flow cases utilises periodic boundary conditions on two sets of planes: spanwise and streamwise planes.

The first thing to do when simulating a double periodic channel flow problem is to determine the requirement of the channel flow domain size. The size of the domain must be meticulously determined to minimise the computational expenses but ensuring all of the necessary turbulence structures are captured appropriately. The minimum size of the double periodic channel flows are commonly referred as the minimal flow unit [50], shown in Figure 4.

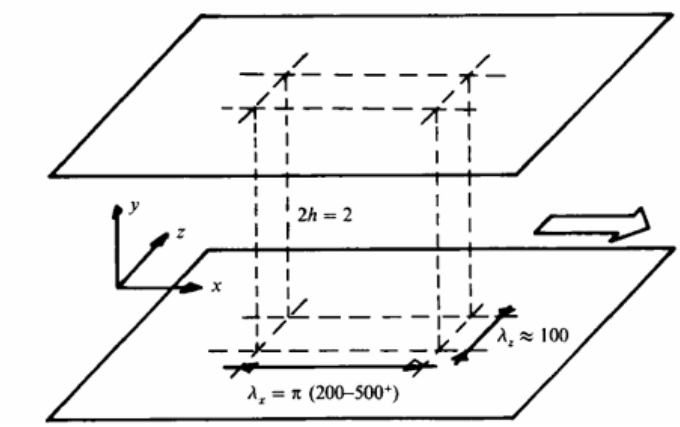

Figure 4: Minimal Flow Unit of a Double Periodic Channel Flow [50]

The length of the minimal flow unit is defined in a wall flow unit, denoted by the (+) sign. The (+) sign is a normalisation of quantities using the viscous length scale, formulated as:

$$\delta_\nu = \frac{\nu}{u_\tau} \tag{8}$$

Where u_τ is a function of wall friction, defined as [51]:

$$u_\tau = \sqrt{\frac{\tau_w}{\rho}} \tag{9}$$

τ_w is related to the Reynolds numbers and the velocity gradient to the normal direction, stated as [52]:

$$\tau_w = \frac{\partial u}{\partial y} Re \tag{10}$$

Re is the dimensionless number which displays the ratio between the inertial and viscous forces, expressed as [53]:

$$Re = \frac{v\delta}{\nu} \tag{11}$$

For study in turbulence, friction Reynolds numbers are more commonly used due to its relevance to the near wall turbulence. The equation of the friction Reynolds number is displayed below [51].

$$Re_\tau = \frac{u_\tau \delta}{\nu} \approx 0.09(2Re)^{0.88} \tag{12}$$

For the base case, the Reynolds number are defined as $Re_\tau = 180$. The quantity is chosen due to the availability of DNS channel flow data [54] and the data from Xcompact3D [42]. The fluid properties data is shown in the Table 3 below.

Table 3: Fluid Properties

Re_τ	Re	u_b	ρ	ν
180	2819.294	1	1	0.00035

2.2 Theoretical Background

2.2.1 Governing Equations of Incompressible Fluid Flow

In a low Reynolds number case such as defined in Section **??**, the fluid becomes incompressible, which transforms both governing equations of the fluid flow [55]. For the continuity equation, the expression simplifies into:

$$\nabla \mathbf{u} = 0 \tag{13}$$

The bold variables denotes a field. For the context of $\mathbf{u}$, which is the velocity field, it can be expanded into:

$$\mathbf{u} = u\mathbf{e_x} + v\mathbf{e_y} + w\mathbf{e_z} \tag{14}$$

On the other hand, the momentum equation changes by dropping the compressibility term. Moreover, because of no height change involved in the channel flow, the gravity term is also dropped. Additionally, the momentum equation can be modified by normalising every term to density, as density remains constant in incompressible flow.

$$\underbrace{\frac{\partial \mathbf{u}}{\partial t}}_{\text{I.}} + \underbrace{(\mathbf{u} \cdot \nabla)\mathbf{u}}_{\text{II.}} = \underbrace{-\frac{1}{\rho}\nabla p}_{\text{III.}} + \underbrace{\nu \nabla^2 \mathbf{u}}_{\text{IV.}} \tag{15}$$

There are four members in a incompressible Navier-Stokes equation. The term I is the unsteady term, showing the change of the fluid velocity over time. The term II is the convective term, showing the transport of properties in the flow. The third term is the pressure gradient, showing the change of pressure in the fluid. Lastly, term IV, determines how the viscous diffusion and dissipation affecting the flow.

2.2.2 Fractional Step Method

In incompressible flow, the density remains constant while the pressure changes. Therefore, the equation of state is not applicable [55], hence pressure and velocity equation must be calculated together in a coupled equation. In Xcompact3D, the Fractional Step Method is used [56]. In Fractional Step method, there are four steps that is conducted to couple the pressure and velocity variables [57]. The first step utilises intermediate velocity field,

which is expressed as [58]:

$$\frac{\hat{\mathbf{u}}^k - \mathbf{u}^{k-1}}{\Delta t} = \gamma_k \mathcal{A}(\mathbf{u}^{k-1}) + \theta_k \mathcal{A}(\mathbf{u}^{k-2}) - \alpha_k \nabla p^{k-1} \tag{16}$$

Where $\mathcal{A}$ is the convection-diffusion operator, which includes both terms II and IV of the Navier-Stokes equations [16]. It also worth noting that the intermediate velocity field does not satisfy the continuity equation due to its divergence-free characteristics.

Then, the second step is to solve the predicted scalar field, using the following relation:

$$\nabla^2 \phi^k = \frac{1}{\alpha_k \Delta t} \nabla \hat{\mathbf{u}}^k \tag{17}$$

This step is based on the pressure-Poisson equation, which makes this step computationally demanding [16]. Therefore, 3D FFT scheme is used to solve the scalar field equation [59].

The third step is to update the velocity using the known scalar field and intermediate velocity field.

$$\mathbf{u}^k = \hat{\mathbf{u}}^k - \alpha_k \Delta t \nabla \phi^k \tag{18}$$

Finally, the pressure field is updated using the relation with the scalar field:

$$p^k = p^{k-1} + \phi^k \tag{19}$$

2.2.3 Spatial Discretisation

Solving the Navier-Stokes equation numerically requires spatial discretisation, which involves transferring the properties of the flow from one member to another [60]. Xcompact3d uses various types of compact finite difference schemes [44], due to its ability to solve the derived values of a defined point and the neighbouring members simultaneously. This study uses the 6th-order centred Hermitian compact scheme, which solved the first derivation of the values as: [61]:

$$\alpha \mathbf{u}'_{i-1} + \mathbf{u}'_i + \alpha \mathbf{u}'_{i+1} = a \frac{\mathbf{u}_{i+1} - \mathbf{u}_{i-1}}{2\Delta x} + b \frac{\mathbf{u}_{i+2} - \mathbf{u}_{i-2}}{4\Delta x} \tag{20}$$

For the variables, it is set into $\alpha = 1/3$, $a = 14/9$, and $b = 1/9$ to ensure the scheme can represent a wide range of turbulence scales [44]. The second derivative also uses the 6th-order central scheme, expressed as:

$$\alpha \mathbf{u}''_j + \mathbf{u}''_{j+1} + \alpha \mathbf{u}''_{j+1} = a\frac{\mathbf{u}_{i+1} - 2\mathbf{u}_i + \mathbf{u}_{i-1}}{\Delta x^2} + b\frac{\mathbf{u}_{i+2} - 2\mathbf{u}_i + \mathbf{u}_{i-2}}{4\Delta x^2} + c\frac{\mathbf{u}_{i+3} - 2\mathbf{u}_i + \mathbf{u}_{i-3}}{9\Delta x^2} \tag{21}$$

To ensure the same range as the first derivative, the variables α is set to 2/11, a is set to 12/11, b is set to 3/11, and c is set to 0. Using these equations and the said variables value, the scheme can calculate the results with 4 or 5 times lower number of mesh nodes compared to 2nd order schemes while only increasing 2 times of its computational expenses [56].

2.2.4 Temporal Discretisation

Other than the spatial discretisation, temporal discretisation must also be applied to calculation so the numerical simulation can be progressed to the next time step. For nearly all of the time discretisation, the third-order Adam-Bashforth equation is used. The third order Adam-Bashforth scheme is an explicit scheme that uses one equation to progress the time step of the calculation [62], displayed as:

$$\phi^{n+1} - \phi^n = \frac{\Delta t}{12}[23F^n - 16F^{n+1} + 5F^{n-2}] \tag{22}$$

Where

$$F^n = \mathbf{u}^n\phi^n$$
$$F^{n-1} = \mathbf{u}^{n-1}\phi^{n-1}$$
$$F^{n-2} = \mathbf{u}^{n-2}\phi^{n-2}$$

For the diffusion term in the wall-normal direction, the implicit Crank-Nicolson equation is also used for the time discretisation. The temporal discretisation for the y-diffusion term can be expressed as:

$$\left(\nu\frac{\partial^2 v}{\partial y^2}\right)^{n+\frac{1}{2}} = \frac{1}{2}\left(\nu\frac{\partial^2 v^{n+1}}{\partial y^2} + \nu\frac{\partial^2 v^n}{\partial y^2}\right) \tag{23}$$

2.3 Computational Procedures

2.3.1 Xcompact3d Setup

Xcompact3d, as any other FORTRAN F90 based code, must be downloaded and compiled before being able to be used as an analysis software. The code is downloaded through its official Github repository, using:

```
git clone https://github.com/xcompact3d/Incompact3d
```

After that, the code is compiled using the following commands on unix, assuming 8 threads are available for compiling the code:

```
cd Incompact3d
export FC=mpif90
cmake -S . -B build
cd build
cmake --build . -j 8
```

Then by going to the *input.i3d* file in each example code, the boundary conditions, as well as domain size, number of mesh, and initial condition can be changed.

2.3.2 Grid Generation

For the entirety of the study, the cartesian structured grid is used. The entire model is discretised into a system of hexahedral-shaped elements with eight nodes connecting to each other [63]. In a simple canonical flow as this study, the structured hexahedral grid is favoured due to the the efficiency of the shape in terms of filling the spaces, as well as the ability of minimising diffusion when transfering the properties from an element to another [64]. Additionally, the simple connectivity of the elements makes the grid model simple to program [65].

To capture the near-wall turbulence, the size of the grid near the wall must be decreased. However, just uniformly decrease the size of the grid may cause an unnecessary computational expense as the flow on the centre of the channel flow do not have substantial gradient or turbulence structures. To compensate the problem, a stretching algorithm is introduced in the Xcompact3d program [44], developed from [66] and [67]. First, the domain must be expressed in physical coordinate y and computational coordinate s.

$$y = h(s), 0 \leq s \leq 1, 0 \leq y \leq L_y \tag{24}$$

The y-height of each members can be defined as

$$h = \frac{L_y\sqrt{\beta}}{\gamma\sqrt{\alpha}\sqrt{\alpha\beta}+1}\left\{\tan^{-1}\left(\frac{\sqrt{\alpha\beta}+1\tan(\pi(\gamma s+\delta))}{\sqrt{\alpha}\sqrt{\beta}}\right)+\pi\left[H\left(s-\frac{1-2\delta}{2\gamma}\right)+H\left(s-\frac{3-2\delta}{2\gamma}\right)\right]-\tan^{-1}\left(\frac{\sqrt{\alpha\beta}+1\tan(\pi\delta)}{\sqrt{\alpha}\sqrt{\beta}}\right)\right\} \tag{25}$$

On a default channel case in Xcompact3d, the refinement are conducted solely for the wall. Therefore, $\gamma = 1$ and $\delta = \frac{1}{2}$. For all the case, β is set to 0.259065151.

2.3.3 Channel Flow Generalised Richardson Extrapolation Campaign

In order to conduct the Generalised Richardson Extrapolation, several channel flow models must be generated with spatial, temporal, and domain size variation. The variation of the simulation models are shown in Table 4.

Table 4: Simulation Model Variation

Mesh Type	Finest	Fine	Medium	Coarse
L_x	8π	4π	2π	π
L_y	2	2	2	2
L_z	3π	1.5π	0.75π	0.375π
N_x	1024	256	64	16
N_y	1021	509	256	128
N_z	1024	256	64	16
$N_{t,spinup}$	35000	35000	35000	35000
$N_{t,warmup}$	40000	40000	40000	40000
$N_{t,sampling}$	200000	50000	12500	3125
Δt	0.001	0.002	0.004	0.008
t_{tot}	200	100	50	25

Processing the result of the model variation requires a normalised resolution value so the difference in value can be consistently compared. For that, a normalised resolution is introduced as:

$$NR = \frac{\Delta x_e^{current}}{\Delta x_e^{finest}} \frac{\Delta t^{current}}{\Delta t^{finest}} \frac{t_{tot}^{finest}}{t_{tot}^{current}} \frac{L_e^{finest}}{L_e^{current}} \tag{26}$$

Where

$$\Delta x_e = \sqrt[3]{\frac{L_x L_y L_z}{N_x N_y N_z}} \tag{27}$$

$$L_e = \sqrt[3]{L_x L_y L_z} \tag{28}$$

2.3.4 Oscillating Wall Generalised Richardson Extrapolation

Simulating the oscillating wall requires a slight change to the wall boundary condition. By default, the wall is set into a no-slip condition. Therefore, the boundary condition needs to be modified so the wave equation can be included in the wall boundary condition. The base wave equation for the oscillating wall is:

$$w(x,t) = A\sin(2\pi\omega t) \tag{29}$$

For the ease of actuation adjustment in different Reynolds number, the wave parameters are non-dimensionalised with wall-normal values [22]. The dimensionless variables required are

$$A^+ = A/u_\tau \tag{30}$$

$$T^+ = 2\pi \frac{u_\tau^2}{\omega\nu} \tag{31}$$

$$k_x^+ = k_x \frac{\nu}{u_\tau} \tag{32}$$

The values of the wall-normalised parameters are based on past studies [9] [68], tabulated in Table 5.

Table 5: Oscillation Parameters Variation

Re	T_{osc}^+	A^+	k_x^+
180	100	4.9	0.0014

For the oscillating wall boundary condition problem, the code must be modified first before compiling, especially for the Navier-Stokes solver, which is named navier.f90. In the said file, the wall z-velocities *uz* for both walls in *pres_correc* subroutine are changed into the defined wall wave function. In this case, the code was modified into:

```
!********NCLY==2************************************
if (ncly1==2) then
if (xstart(2)==1) then
do k=1,xsize(3)
do i=1,xsize(1)
dpdxy1(i,k)=dpdxy1(i,k)*gdt(itr)
dpdzy1(i,k)=dpdzy1(i,k)*gdt(itr)
enddo
enddo
do k=1,xsize(3)
do i=1,xsize(1)
ux(i,1,k)=byx1(i,k)+dpdxy1(i,k)
uy(i,1,k)=byy1(i,k)
uz(i,1,k)=0.31814*sin(2*3.14159*11.18310*t)
enddo
enddo
```

```
endif
endif

if (nclyn==2) then
if (xend(2)==ny) then
do k=1,xsize(3)
do i=1,xsize(1)
dpdxyn(i,k)=dpdxyn(i,k)*gdt(itr)
dpdzyn(i,k)=dpdzyn(i,k)*gdt(itr)
enddo
enddo
endif
if (dims(1)==1) then
do k=1,xsize(3)
do i=1,xsize(1)
ux(i,xsize(2),k)=byxn(i,k)+dpdxyn(i,k)
uy(i,xsize(2),k)=byyn(i,k)
uz(i,xsize(2),k)=0.31814*sin(2*3.14159*11.18310*t)
enddo
enddo
elseif (ny - (nym / dims(1)) == xstart(2)) then
do k=1,xsize(3)
do i=1,xsize(1)
ux(i,xsize(2),k)=byxn(i,k)+dpdxyn(i,k)
uy(i,xsize(2),k)=byyn(i,k)
uz(i,xsize(2),k)=0.31814*sin(2*3.14159*11.18310*t)
enddo
enddo
endif
endif
```

Understanding and quantifying the efficiency of the flow control method is in utmost importance for this analysis. To calculate the efficiency, the drag reduction is priorly measured using:

$$DR = \frac{\tau_{w,CF} - \tau_{w,osc}}{\tau_{w,CF}} = \frac{p_{CF} - p_{osc}}{p_{CF}} \tag{33}$$

For the net power saving, it is calculated using [9]:

$$NPS = DR - p_{in} \tag{34}$$

Where p_{in} can be calculated using:

$$p_{in} = \frac{1}{p_{CF} T_{av} L_x L_y} \int_{t_i}^{t_f} \int_0^{L_x} \int_0^{L_z} W \tau_z dx dz dt \tag{35}$$

3 Results and Discussion

3.1 Channel Flow Results

3.1.1 Grid Convergence Study and Generalised Richardson Extrapolation Result

A parameter of the simulation results is used to determine the ideal and converged simulation result using the Generalised Richardson Extrapolation. Coefficient of friction parameter in various resolutions are used in the grid convergence study, with the results shown in the Figure 2.3.

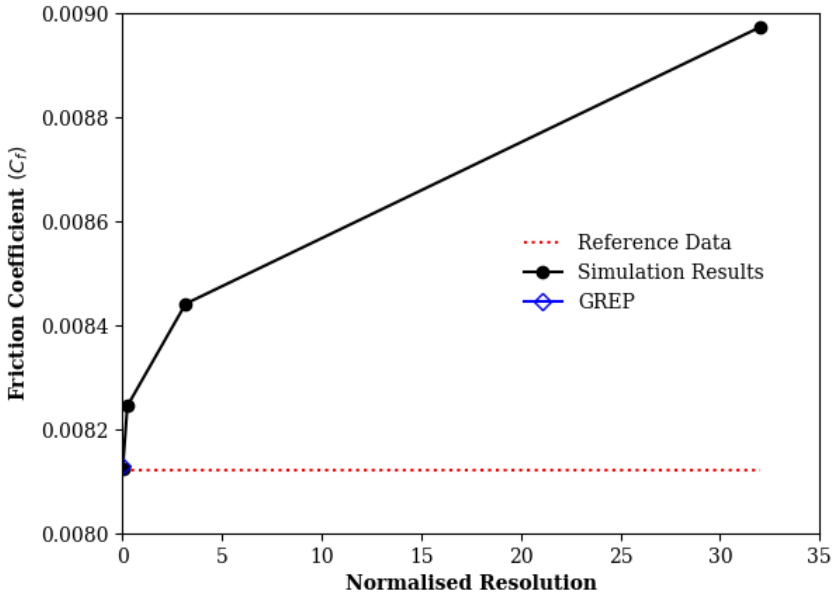

Figure 5: Grid Convergence Study with Generalised Richardson Extrapolation

Based on the results, it is apparent that the resolution values are already sufficient to show a converging value in the channel flow simulations. Additionally, the value is converging to the reference data given [69]. with the fine resolution already quite close the reference data. This is a promising result as it can suggest that the fine resolution values are adequate to simulate channel flows at $Re_\tau = 180$, decreasing the computational requirement.

For the Generalised Richardson extrapolation, the result is nearly identical to the reference data and the finest mesh resolution, only yields to 0.00093 % difference to the reference value and 0.00046 % error to the finest mesh resolution. Therefore, the proposed Generalised Richardson Extrapolation can be deemed as valid and sufficient model to predict the values of channel flow simulation in an idealised state.

3.1.2 Mean Streamwise Velocity

Figure 6 displays the mean streamwise velocity of the channel flow normalised to the viscous length scale. The result is as expected, as the value of the velocities becomes closer to the reference data [69].

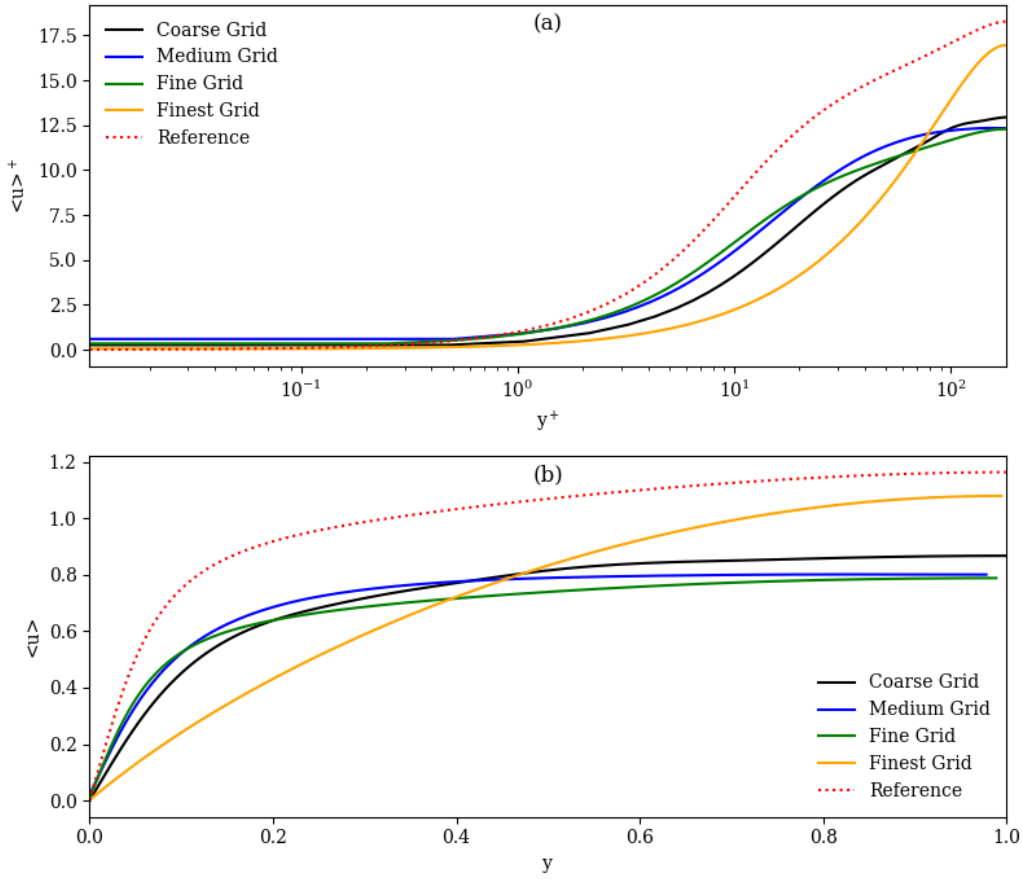

Figure 6: Mean Streamwise Velocity (a) as a Function of Viscous Length Scale and (b) As It Is, on the First Half of the Height of the Channel Flow. The Reference Data Corresponds with Lee and Moser Channel Flow Data [69]

The finest mesh model is the only mesh model that has values close to the reference values, showing only 1.02% difference on the maximum velocity. However, in the overall values, the finest mesh models displays different trend of of streamwise velocity compared to the other mesh models, as well as the reference values. The difference can be understood by analysing the streamwise velocity profile changes in the channel flow, shown in Figure 7.

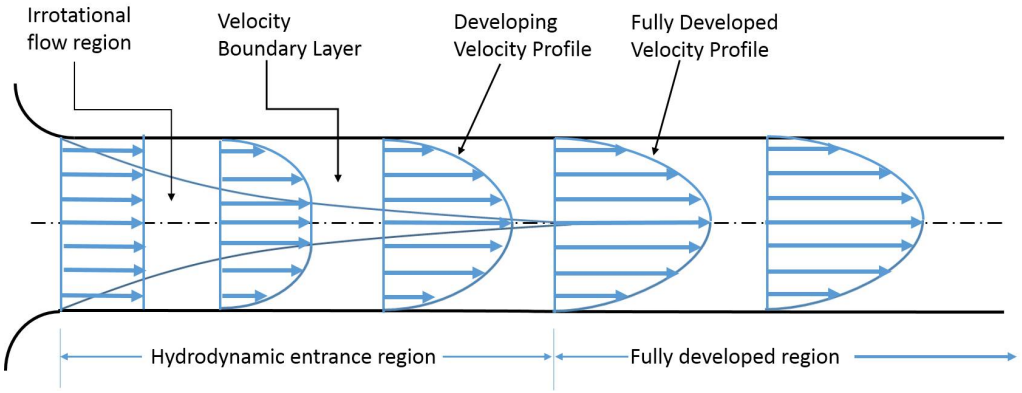

Figure 7: Streamwise Velocity Profile Changes in a Channel Flow [70]

The finest mesh models shows a fully developed velocity profile, while the other models shows a velocity trend that mimics a flow with developing boundary layers. This is caused by the long iteration time. This gives the boundary layer more time to fully develop, thus gives the different trend of velocity profile.

3.1.3 Reynolds Stresses

3.1.4 Velocity Distribution

3.1.5 Pressure and Moment Coefficients

3.2 Viscous Flow

3.3 Off-Design Conditions

4 Conclusions and Recommendations

4.1 Conclusions

4.2 Recommendations for Future Work

References

[1] E. Douglas, J. Jacobs, K. Hayhoe, *et al.*, "Progress and challenges in incorporating climate change information into transportation research and design," *Journal of Infrastructure Systems*, vol. 23, no. 4, p. 04 017 018, 2017. DOI: 10.1061/(ASCE)IS.1943-555X.0000377. eprint: https://ascelibrary.org/doi/pdf/10.1061/%28ASCE%29IS.1943-555X.0000377. [Online]. Available: https://ascelibrary.org/doi/abs/10.1061/%28ASCE%29IS.1943-555X.0000377.

[2] Met Office, *Causes of climate change*. [Online]. Available: https://www.metoffice.gov.uk/weather/climate-change/causes-of-climate-change.

[3] IRENA, *Investment Needs of USD 35 trillion by 2030 for Successful Energy Transition*, 2023. [Online]. Available: https://www.irena.org/News/pressreleases/2023/Mar/Investment-Needs-of-USD-35-trillion-by-2030-for-Successful-Energy-Transition.

[4] IEA, *Tracking clean energy progress 2023*. [Online]. Available: https://www.iea.org/reports/tracking-clean-energy-progress-2023.

[5] A. Abbas, G. Bugeda, E. Ferrer, *et al.*, "Drag reduction via turbulent boundary layer flow control," *Science China Technological Sciences*, vol. 60, pp. 1281–1290, 9 Sep. 2017, ISSN: 18691900. DOI: 10.1007/s11431-016-9013-6.

[6] C. Airiau, R. King, and B. R. Noack, *Open invited track : Flow control strategies and applications*, 2016.

[7] R. Benzi and F. Toschi, "Lectures on turbulence," *Physics Reports*, vol. 1021, pp. 1–106, Jun. 2023, ISSN: 03701573. DOI: 10.1016/j.physrep.2023.05.001.

[8] W. Bell, "The influence of turbulence on drag," *Ocean Engineering*, vol. 6, pp. 329–340, 3 Jan. 1979, ISSN: 00298018. DOI: 10.1016/0029-8018(79)90021-0.

[9] I. Marusic, D. Chandran, A. Rouhi, *et al.*, "An energy-efficient pathway to turbulent drag reduction," *Nature Communications*, vol. 12, 1 Dec. 2021, ISSN: 20411723. DOI: 10.1038/s41467-021-26128-8.

[10] T. Alberti, R. Benzi, and V. Carbone, "Why (still) studying turbulence in fluids and plasmas?" *Perspectives of Earth and Space Scientists*, vol. 4, 1 Dec. 2023, ISSN: 2637-6989. DOI: 10.1029/2023cn000215.

[11] S. Chen, S. Sammak, P. Givi, J. P. Yurko1, and X. Jia, "Reconstructing high-resolution turbulent flows using physics-guided neural networks," Sep. 2021. [Online]. Available: http://arxiv.org/abs/2109.03327.

[12] K. R. Sreenivasan, "Fluid turbulence," *Reviews of Modern Physics*, vol. 71, pp. 383–395, 2 1999.

[13] A. K. F. Hussain, "Coherent structures and turbulence," *Journal of Fluid Mechanics*, vol. 173, pp. 303–356, 1986, ISSN: 14697645. DOI: 10.1017/S0022112086001192.

[14] H. E. Fiedler, "Coherent structures in turbulent flows," *Prog. Aerospace Sci.*, vol. 25, pp. 231–269, 1988.

[15] Y. Wang, W. Huang, and C. Xu, "On hairpin vortex generation from near-wall streamwise vortices," *Acta Mechanica Sinica/Lixue Xuebao*, vol. 31, pp. 139–152, 2 May 2015, ISSN: 05677718. DOI: 10.1007/s10409-015-0415-8.

[16] T. I. Józsa, *Drag reduction by passive in-plane wall motions in turbulent wall-bounded flows[ph.d thesis]*, 2019.

[17] G. Alfonsi, "Coherent structures of turbulence: Methods of eduction and results," *Applied Mechanics Reviews*, vol. 59, pp. 307–323, 1-6 2006, ISSN: 00036900. DOI: 10.1115/1.2345370.

[18] Y. Fan and W. Li, "Spectral analysis of turbulence kinetic and internal energy budgets in hypersonic turbulent boundary layers," *Phys. Rev. Fluids*, vol. 8, p. 044 604, 4 Apr. 2023. DOI: 10.1103/PhysRevFluids.8.044604. [Online]. Available: https://link.aps.org/doi/10.1103/PhysRevFluids.8.044604.

[19] C. Brennen, "Turbulence spectra and scales," in California Institute of Technology, 2004.

[20] T. Kalmár-Nagy and B. D. Bak, "An intriguing analogy of kolmogorov's scaling law in a hierarchical mass–spring–damper model," *Nonlinear Dynamics*, vol. 95, pp. 3193–3203, 4 Mar. 2019, ISSN: 0924-090X. DOI: 10.1007/s11071-018-04749-x.

[21] M. Jahamiri, *Active flow control: A review*, 2010.

[22] P. Ricco, M. Skote, and M. A. Leschziner, "A review of turbulent skin-friction drag reduction by near-wall transverse forcing," *Progress in Aerospace Sciences*, vol. 123, May 2021, ISSN: 03760421. DOI: 10.1016/j.paerosci.2021.100713.

[23] D. Gatti and M. Quadrio, "Reynolds-number dependence of turbulent skin-friction drag reduction induced by spanwise forcing," *Journal of Fluid Mechanics*, vol. 802, pp. 553–582, Sep. 2016, ISSN: 14697645. DOI: 10.1017/jfm.2016.485.

[24] M. Quadrio, P. Ricco, and C. Viotti, "Streamwise-travelling waves of spanwise wall velocity for turbulent drag reduction," *Journal of Fluid Mechanics*, vol. 627, pp. 161–178, 2009, ISSN: 14697645. DOI: 10.1017/S0022112009006077.

[25] F. Auteri, A. Baron, M. Belan, G. Campanardi, and M. Quadrio, "Experimental assessment of drag reduction by traveling waves in a turbulent pipe flow," *Physics of Fluids*, vol. 22, 115103 Aug. 2010. DOI: 10.1063/1.3491203. [Online]. Available: http://arxiv.org/abs/1008.2584%20http://dx.doi.org/10.1063/1.3491203.

[26] C. Viotti, M. Quadrio, and P. Luchini, "Streamwise oscillation of spanwise velocity at the wall of a channel for turbulent drag reduction," *Physics of Fluids*, vol. 21, pp. 1–9, 11 2009, ISSN: 10706631. DOI: 10.1063/1.3266945.

[27] D. Chandran, A. Zampiron, A. Rouhi, *et al.*, "Turbulent drag reduction by spanwise wall forcing. part 2. high-reynolds-number experiments," *Journal of Fluid Mechanics*, vol. 968, Jul. 2023, ISSN: 14697645. DOI: 10.1017/jfm.2023.498.

[28] R. Deshpande, A. G. Kidanemariam, and I. Marusic, "Pressure drag reduction via imposition of spanwise wall oscillations on a rough wall," *Journal of Fluid Mechanics*, vol. 979, Jan. 2024, ISSN: 0022-1120. DOI: 10.1017/jfm.2023.1062.

[29] V. T. Nguyen, P. Ricco, and G. Pironti, "Separation drag reduction through a spanwise oscillating pressure gradient," *Journal of Fluid Mechanics*, vol. 912, 2021, ISSN: 14697645. DOI: 10.1017/jfm.2020.1124.

[30] P. Ricco, C. Ottonelli, Y. Hasegawa, and M. Quadrio, "Changes in turbulent dissipation in a channel flow with oscillating walls," *Journal of Fluid Mechanics*, vol. 700, pp. 77–104, Jun. 2012, ISSN: 14697645. DOI: 10.1017/jfm.2012.97.

[31] D. D. Apsley, *Flow in Pipes and Channels [Lecture Notes]*, 2023. [Online]. Available: https://personalpages.manchester.ac.uk/staff/david.d.apsley/lectures/hydraulics2/t2.

[32] The TrEnCh Project, "Turbulence and fluid flow," in University of Washington, 2023.

[33] K. Duraisamy, G. Iaccarino, and H. Xiao, "Turbulence modeling in the age of data," *Annual Review of Fluid Mechanics*, vol. 51, pp. 357–377, 1 Jan. 2019, ISSN: 0066-4189. DOI: 10.1146/annurev-fluid-010518-040547.

[34] N. A. C. Sidik, S. N. A. Yusuf, Y. Asako, S. B. Mohamed, and W. M. A. A. Japa, "A short review on rans turbulence models," *CFD Letters*, vol. 12, pp. 83–96, 11 Nov. 2020, ISSN: 21801363. DOI: 10.37934/cfdl.12.11.8396.

[35] R. H. Bush, T. Chyczewski, K. Duraisamy, B. Eisfeld, C. L. Rumsey, and B. R. Smith, *Recommendations for future efforts in rans modeling and simulation*, 2020.

[36] Y. Zhiyin, "Large-eddy simulation: Past, present and the future," *Chinese Journal of Aeronautics*, vol. 28, pp. 11–24, 1 Feb. 2015, ISSN: 10009361. DOI: 10.1016/j.cja.2014.12.007.

[37] P. Mason, "Large-eddy simulation: A critical review of the technique," *Quarterly Journal of Royal Meteorological Society*, vol. 120, pp. 1–26, 1994.

[38] P. Moin and K. Mahesh, "Direct numerical simulation: A tool in turbulence research," *Annual Review of Fluid Mechanics*, vol. 30, pp. 539–578, 1998, ISSN: 00664189. DOI: 10.1146/annurev.fluid.30.1.539.

[39] J. Boschung, F. Hennig, M. Gauding, H. Pitsch, and N. Peters, "Generalised higher-order kolmogorov scales," *Journal of Fluid Mechanics*, vol. 794, pp. 233–251, May 2016, ISSN: 14697645. DOI: 10.1017/jfm.2016.172.

[40] P. Roache, "Verification and validation in computational science and engineering," *Journal of Computational Physics*, vol. 123, no. 4, pp. 567–589, 2009.

[41] C. E. Groves, M. Ilie, and P. Schallhorn, *Comprehensive approach to verification and validation of cfd simulations applied to backward facing step - application of cfd uncertainty analysis*, 2012.

[42] P. Bartholomew, G. Deskos, R. A. Frantz, F. N. Schuch, E. Lamballais, and S. Laizet, "Xcompact3d: An open-source framework for solving turbulence problems on a cartesian mesh," *SoftwareX*, vol. 12, Jul. 2020, ISSN: 23527110. DOI: 10.1016/j.softx.2020.100550.

[43] S. Laizet, "Incompact3d: A powerful tool to tackle turbulence problems on supercomputers," T. Kvamsdal, Ed., 2014. [Online]. Available: http://www3.imperial.ac.uk/tmfc/people/sylvainlaizet/.

[44] S. Laizet and E. Lamballais, "High-order compact schemes for incompressible flows: A simple and efficient method with quasi-spectral accuracy," *Journal of Computational Physics*, vol. 228, pp. 5989–6015, 16 Sep. 2009, ISSN: 10902716. DOI: 10.1016/j.jcp.2009.05.010.

[45] Cornell University, *Scaling [virtual workshop note]*, 2024. [Online]. Available: https://cvw.cac.cornell.edu/parallel/efficiency/scaling.

[46] X. Li, *Scalability: Strong and weak scaling*, 2018. [Online]. Available: https://www.kth.se/blogs/pdc/2018/11/scalability-strong-and-weak-scaling/.

[47] G. M. Amdahl, "Validity of the single processor approach to achieving large scale computing capabilities," in *Proceedings of the April 18-20, 1967, Spring Joint Computer Conference*, ser. AFIPS '67 (Spring), Atlantic City, New Jersey: Association for Computing Machinery, 1967, pp. 483–485, ISBN: 9781450378956. DOI: 10.1145/1465482.1465560. [Online]. Available: https://doi.org/10.1145/1465482.1465560.

[48] J. L. Gustafson, "Reevaluating amdahl's law," *Commun. ACM*, vol. 31, no. 5, pp. 532–533, May 1988, ISSN: 0001-0782. DOI: 10.1145/42411.42415. [Online]. Available: https://doi.org/10.1145/42411.42415.

[49] EPCC, *Archer2 cu calculator*, 2024. [Online]. Available: https://www.archer2.ac.uk/support-access/cu-calc.html.

[50] J. Jiménez and P. Moin, "The minimal flow unit in near-wall turbulence," *Journal of Fluid Mechanics*, vol. 225, pp. 213–240, 1991. DOI: 10.1017/S0022112091002033.

[51] S. B. Pope, *Turbulent Flows*. Cambridge University Press, 2000.

[52] C. D. Daniel, S. Laizet, and J. C. Vassilicos, "Wall shear stress fluctuations: Mixed scaling and their effects on velocity fluctuations in a turbulent boundary layer," 2017.

[53] N. G. R. Center, *Reynolds number*, 2024. [Online]. Available: https://www.grc.nasa.gov/www/k-12/airplane/reynolds.html.

[54] M. Lee and R. D. Moser, "Direct numerical simulation of turbulent channel flow up to," *Journal of Fluid Mechanics*, vol. 774, pp. 395–415, Jul. 2015, ISSN: 0022-1120. DOI: 10.1017/jfm.2015.268.

[55] L. Könözsy, *Numerical Methods for Incompressible Flows [Course Notes]*, Canvas Cranfield, 2024.

[56] S. Laizet, *XCompact3d Introduction [Course Slide]*, Xcompact3d Course, 2024.

[57] D. G. Westra and J. C. Heinrich, *The fractional step method applied to simulations of natural convective flows*, 2002.

[58] J. van Kan, "A second-order accurate pressure-correction scheme for viscous incompressible flow," *SIAM Journal on Scientific and Statistical Computing*, vol. 7, no. 3, pp. 870–891, 1986. DOI: 10.1137/0907059. eprint: https://doi.org/10.1137/0907059. [Online]. Available: https://doi.org/10.1137/0907059.

[59] N. Li and S. Laizet, "2decompfft - a highly scalable 2d decomposition library and fft interface," in *Cray User Group*, 2010, pp. 1–13.

[60] H. K. Hawez, R. Sanaee, and N. H. Faisal, "A critical review on coupled geomechanics and fluid flow in naturally fractured reservoirs," *Journal of Natural Gas Science and Engineering*, vol. 95, p. 104 150, 2021, ISSN: 1875-5100. DOI: https://doi.org/10.1016/j.jngse.2021.104150. [Online]. Available: https://www.sciencedirect.com/science/article/pii/S1875510021003516.

[61] S. Laizet, *INCOMPACT 3D USER GUIDE version2.0 [User Guide]*, 2024. [Online]. Available: https://www.incompact3d.com/uploads/5/8/7/2/58724623/_user_guide_incompact3d_v2.pdf.

[62] D. R. Durran, "The third-order adams-bashforth method: An attractive alternative to leapfrog time differencing," *Monthly Weather Review*, vol. 119, pp. 702–720, 3 1991.

[63] G. H. Yeoh and J. Tu, "Solution methods for multi-phase flows," in Elsevier, 2010, pp. 95–242. DOI: 10.1016/B978-0-08-046733-7.00003-5.

[64] Ansys, *ANSYS Fluent Mosaic Technology Automatically Combines Disparate Meshes with Polyhedral Elements for Fast, Accurate Flow Resolution [White Paper]*, 2020.

[65] J. Tu, G.-H. Yeoh, and C. Liu, "Chapter 4 - cfd mesh generation: A practical guideline," in *Computational Fluid Dynamics (Third Edition)*, J. Tu, G.-H. Yeoh, and C. Liu, Eds., Third Edition, Butterworth-Heinemann, 2018, pp. 125–154, ISBN: 978-0-08-101127-0. DOI: https://doi.org/10.1016/B978-0-08-101127-

0.00004-0. [Online]. Available: https://www.sciencedirect.com/science/article/pii/B9780081011270000040.

[66] A. Cain, J. Ferziger, and W. Reynolds, "Discrete orthogonal function expansions for non-uniform grids using the fast fourier transform," *Journal of Computational Physics*, vol. 56, pp. 272–286, 2 Nov. 1984, ISSN: 00219991. DOI: 10.1016/0021-9991(84)90096-2.

[67] E. J. Avital, N. D. Sandham, and K. H. Luo, "Stretched cartesian grids for solution of the incompressible navier-stokes equations," *International Journal for Numerical Methods in Fluids*, vol. 33, pp. 897–918, 6 Jul. 2000, ISSN: 02712091. DOI: 10.1002/1097-0363(20000730)33:6<897::AID-FLD37>3.0.CO;2-4.

[68] D. Zhou and K. S. Ball, "Turbulent drag reduction by spanwise wall oscillations," *International journal of engineering. Transactions A: basics*, vol. 21, pp. 85–104, 2008. [Online]. Available: https://api.semanticscholar.org/CorpusID:17940071.

[69] M. Lee and R. D. Moser, "Direct numerical simulation of turbulent channel flow up to $Re_\tau \approx 5200$," *Journal of Fluid Mechanics*, vol. 774, pp. 395–415, 2015. DOI: 10.1017/jfm.2015.268.

[70] Y. A. Cengel and J. M. Cimbala, *Fluid Mechanics: Fundamentals and Applications*, 4th. McGraw-Hill, Jan. 2019.

APPENDIX

A Software Choice

Software	Advantages	Disadvantages
Incompact3d	DNS is default	Code structure is harder to read, harder interface
	Written in Fortran, less time to familiarise	Hard to find the documentation, contact must be done through Prof. Laizet
	Collaboration with Ricardo	
OpenFOAM	Code structure is easier to read, better interface	Written in C++, requires additional familiarisation time
	Documentation and guidance is already provided by Tom, easier contact if confused	DNS is harder to set up (requires dnsFoam), a lot of files to set up
		No collaboration?